

ISSN: (Print) (Online) Journal homepage: <https://www.tandfonline.com/loi/gcoo20>

# Chemical, physical, and biological properties of Pd(II), V(IV)O, and Ag(I) complexes of N<sub>3</sub> tridentate pyridine-based Schiff base ligand

L. H. Abdel-Rahman , A. M. Abu-Dief , F. M. Atlam , A. A. H. Abdel-Mawgoud ,  
A. A. Alothman , A. M. Alsalme & A. Nafady

To cite this article: L. H. Abdel-Rahman , A. M. Abu-Dief , F. M. Atlam , A. A. H. Abdel-Mawgoud ,  
A. A. Alothman , A. M. Alsalme & A. Nafady (2020) Chemical, physical, and biological properties of  
Pd(II), V(IV)O, and Ag(I) complexes of N<sub>3</sub> tridentate pyridine-based Schiff base ligand, Journal of  
Coordination Chemistry, 73:23, 3150-3173, DOI: [10.1080/00958972.2020.1842378](https://doi.org/10.1080/00958972.2020.1842378)

To link to this article: <https://doi.org/10.1080/00958972.2020.1842378>




View supplementary material 



Published online: 16 Nov 2020.



Submit your article to this journal 



Article views: 18



View related articles 



View Crossmark data 



## Chemical, physical, and biological properties of Pd(II), V(IV)O, and Ag(I) complexes of N<sub>3</sub> tridentate pyridine-based Schiff base ligand

L. H. Abdel-Rahman<sup>a</sup>, A. M. Abu-Dief<sup>a</sup>, F. M. Atlam<sup>b</sup>, A. A. H. Abdel-Mawgoud<sup>a</sup>,  
A. A. Alothman<sup>c</sup>, A. M. Alsalmeh<sup>c</sup> and A. Nafady<sup>c</sup>

<sup>a</sup>Chemistry Department, Faculty of Science, Sohag University, Sohag, Egypt; <sup>b</sup>Department of Chemistry, Faculty of Science, Tanta University, Tanta, Egypt; <sup>c</sup>Department of Chemistry, College of Science, King Saud University, Riyadh, Saudi Arabia

### ABSTRACT

A new N<sub>3</sub>-tridentate imine ligand, 2,6-diacetylpyridinediphenylhydrazone (DAPH) (L), and its Pd(II), V(IV)O, and Ag(I) complexes were synthesized and characterized *via* elemental analysis, FT-IR, NMR, molar conductance, and magnetic susceptibility measurements. The obtained data confirmed geometrical structures of Pd(II), Ag(I), and V(IV)O complexes as square planar, tetrahedral, and distorted square pyramidal, respectively. Minimum inhibitory concentrations (MIC) were used to probe *in vitro* antimicrobial activity of DAPH ligand and metal complexes using three different bacteria. Results revealed that PdDAPH complex exhibited the highest toxicity and lowest MIC (1.25 µg/mL) toward *Escherichia coli*. Moreover, cytotoxic activity of the prepared complexes was evaluated *via* three human cancer cell lines, hepatic carcinoma (HepG2), breast carcinoma (MCF-7), and colon carcinoma (HCT-116). Among all tested complexes, PdDAPH caused a significant loss of cell viability in less time and lower dose than the reference drug vinblastine. Antioxidant activity was also measured for all complexes and compared to vitamin C. Probing the interaction of the prepared metal-DAPH chelates with calf-thymus DNA showed the Pd(II) complex displayed the strongest interaction, with a binding constant of 6.02 kcal mol<sup>-1</sup>. Molecular docking was also investigated on all complexes, with PdDAPH being the most promising compound due to its facile hydrophobic interactions with the active pocket of glucose transporter (GLUT1) enzyme. Overall, the combined findings of this work clearly demonstrate that these new compounds hold promise as efficient antibiotic and anticancer agents.

### ARTICLE HISTORY

Received 26 June 2019  
Accepted 4 October 2020

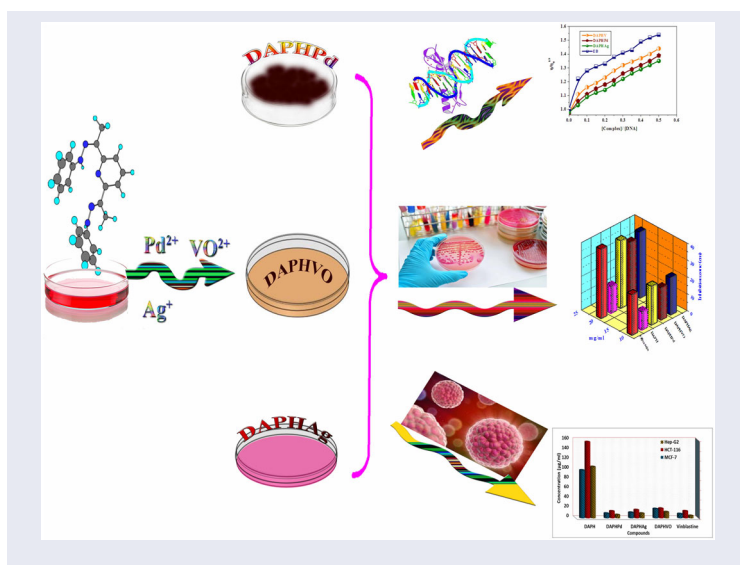
### KEYWORDS

Imine complexes;  
antimicrobial; DNA  
interaction; anticancer;  
antioxidant; docking study

**CONTACT** L. H. Abdel-Rahman ✉ [Lailakenawy@hotmail.com](mailto:Lailakenawy@hotmail.com) Chemistry Department, Faculty of Science, Sohag University, 82524 Sohag, Egypt; A. Nafady ✉ [Anafady@Ksu.edu.sa](mailto:Anafady@Ksu.edu.sa) Department of Chemistry, College of Science, King Saud University, Riyadh 11451, Saudi Arabia

Supplemental data for this article can be accessed [here](#).

© 2020 Informa UK Limited, trading as Taylor & Francis Group



## 1. Introduction

Designing novel drugs with broad-spectrum activity as antimicrobial and anticancer agents is an active field of investigation [1–3]. Much interest has been generated in  $\text{N}_3$ -tridentate imine ligands that have a variety of uses in several domains, depending on molecular structure [4–7]. Understanding the structure/reactivity relationship of these chelators is essential. Moreover, polydentate imine ligands are valuable for their coordination capacity [8], biological activity [9], and metal extraction in analytical chemistry [10]. Minor modifications in ligand structure with hard/soft atoms such as oxygen, sulfur, and nitrogen are expected to affect the chemistry and activity of resultant compounds [11, 12].

Cancer has been considered as one of the leading causes of human mortality worldwide, with more than ten million people dying annually. Many investigations using Schiff-base (imine) ligands coordinated with transition metal ions showed that such complexes possess anticancer activity [11–13]. In particular,  $\text{Pd}(\text{II})$  chelates are used in various applications related to medicine and biology, given their proven antimicrobial, anti-inflammatory, and antitumor properties [14]. Silver sulfadiazine (SSD) has been utilized prophylactically for various bacterial infections. Vanadium acts as a counter ion for proteins (DNA and RNA). Moreover, oxidovanadyl Schiff base chelates are of interest as inhibitors of protein-tyrosine phosphatase 1B and DNA interacting reagents [15]. Although a massive body of work is reported on coordination chemistry and biological activity of Schiff bases with a variety of metal ions [14–18], little information is known about tridentate  $\text{N}_3$ -imine ligands and their metal complexes.

For these reasons and our ongoing research interest on the synthesis of novel Schiff-based ligands and their metal complexes for biological and catalytic applications, we describe, herein, facile procedures for the synthesis and characterization of a new tridentate  $\text{N}_3$ -imine ligand and its  $\text{Pd}(\text{II})$ ,  $\text{V}(\text{IV})\text{O}$ , and  $\text{Ag}(\text{I})$  complexes [13–18].

Spectroscopic and thermal characteristics of chelates along with their biological activity towards selected bacteria, fungi, and cancer cell lines were evaluated. Finally, molecular docking and CT-DNA binding ability were assessed to support biological studies using GLUT1 enzyme, which facilitates the transport of glucose across the plasma membranes of mammalian cells.

## 2. Experimental

### 2.1. Reagents

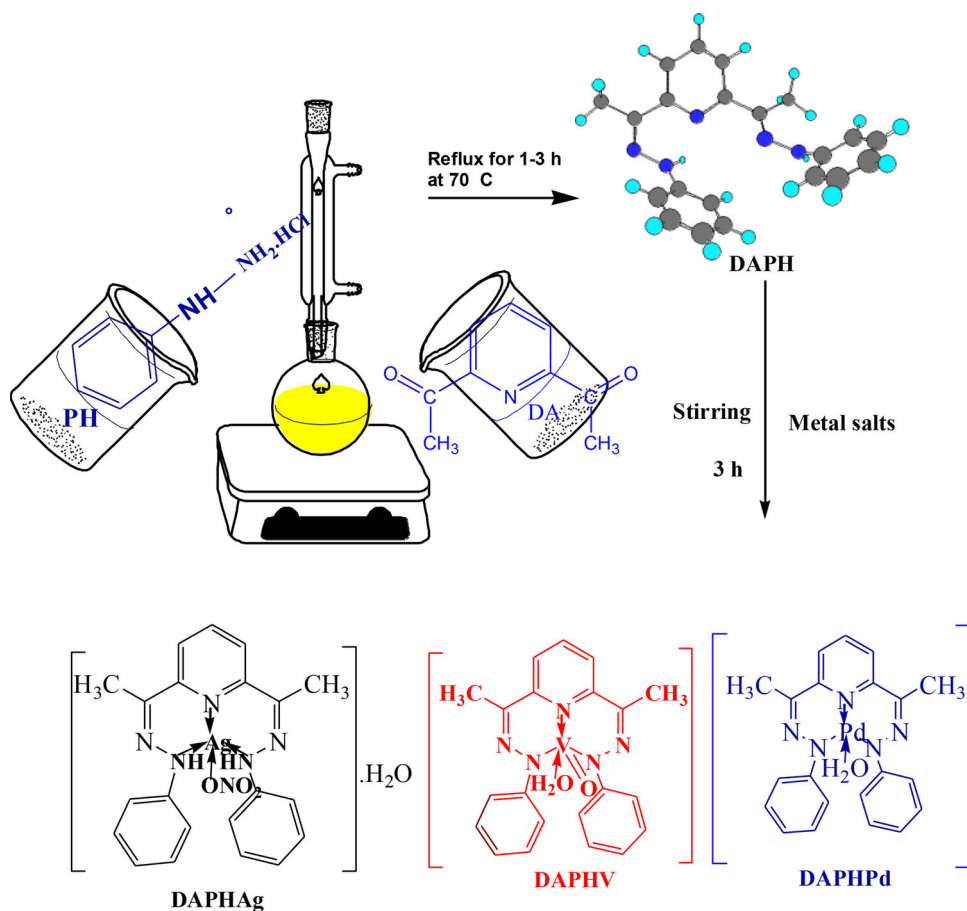
Solvents and main reagents used to synthesize the new ligand and its metal complexes were commercial reagent grade chemicals, applied without purification. 2,6-Diacetylpyridine, phenylhydrazinium chloride, vanadyl acetylacetonate ( $\text{VO}(\text{C}_5\text{H}_7\text{O}_2)_2$ ), silver nitrate ( $\text{AgNO}_3$ ), and palladium acetate ( $\text{Pd}(\text{OAc})_2$ ) were purchased from Sigma-Aldrich Chemie (Munich, Germany). As for DNA binding studies, Sigma-Aldrich solvents such as dimethylformamide (DMF), hydrochloric acid (HCl), ethanol (EtOH), along with calf-thymus DNA (CT-DNA), ethidium bromide (EB), Tris (hydroxymethyl)-aminomethane (Tris), and bromophenol blue dye were employed as received.

### 2.2. Synthesis of imine DAPH ligand

The procedure for preparation of the new ligand was as follows: 5 mmol 2,6-diacetylpyridine (DA, 0.820 g) was dissolved in 10 mL of ethanol and added dropwise under stirring over 5 min at room temperature to a 10 mL methanolic solution of 5 mmol of phenylhydrazinium chloride (PH, 0.545 g). The solid product precipitated after 30 min of stirring and was filtered off, washed, crystallized from ethanol, and dried over anhydrous  $\text{CaCl}_2$ . The yield of the crystalline blood-red imine product (DAPH) was 98%.  $^1\text{H}$  NMR ( $\delta$ , ppm), in  $\text{DMSO-d}_6$ : 9.9–9.4 (b, 2H, 2NH), 8.0–6.86 (m, 13H, aromatic), 2.44 (s, 6H, 2 $\text{CH}_3$ ).  $^{13}\text{C}$  NMR ( $\delta$ , ppm), in  $\text{DMSO-d}_6$ : 145, 129, 120, 118, 113, and 12.

### 2.3. Preparation of PdDAPH, VODAPH, and AgDAPH complexes

New M-DAPH complexes ( $\text{M} = \text{Pd}(\text{II})$ ,  $\text{V}(\text{IV})\text{O}$ , and  $\text{Ag}(\text{I})$ ) were prepared by dropwise mixing of 10 mmol each metal salt (2.24 g of  $\text{Pd}^{2+}$ , 1.69 g of  $\text{Ag}^+$ , and 2.65 g of  $\text{V}^{4+}$ ), dissolved in acetone with 10 mmol (4.17 g) of DAPH ligand in acetone, giving a blood-red solution. The mixture was further stirred for 2 h at  $85^\circ\text{C}$  and left to cool to room temperature. The formed precipitates were filtered off, washed several times with hot water, then with ethanol and diethyl ether. Finally, the isolated metal complexes were dried at room temperature over  $\text{CaCl}_2$ . Attempts to grow single crystals suitable for X-ray crystallographic analysis of all metal-DAPH complexes were unsuccessful, despite the crystalline nature of the DAPH ligand.  $^1\text{H}$  NMR of PdDAPH ( $\delta$ , ppm), in  $\text{DMSO-d}_6$ : 8.01–6.83 (m, 13H, aromatic), 2.43 (s, 6H, 2 $\text{CH}_3$ ).  $^1\text{H}$  NMR of AgDAPH ( $\delta$ , ppm), in  $\text{DMSO-d}_6$ : 9.81–9.79 (b, 2H, 2NH), 8.01–6.85 (m, 13H, aromatic), 2.43 (s, 6H, 2 $\text{CH}_3$ ). The synthetic pathway of the DAPH ligand and its metal complexes is shown in [Scheme 1](#).



**Scheme 1.** Synthetic strategy for preparation of imine complexes.

## 2.4. Analytical and physical characterizations

The melting point of the DAPH ligand, decomposing temperatures of metal complexes, FT-IR, <sup>1</sup>H, and <sup>13</sup>C NMR, UV-Vis spectra in DMF, elemental analyses, and magnetic susceptibility measurements were performed as discussed in our previous work [14–18]. Thermogravimetric analyses were conducted in the air at a heating rate 10 °C min<sup>-1</sup> on a Shimadzu corporation 60 Hz analyzer. Measurements of absorbance of 5 × 10<sup>-3</sup> M chelate solutions were recorded at different pH. An ADWA pH meter with a CL-51B combined electrode was used to measure pH at 298 K after calibration with appropriate buffers (pH 4.02 and pH 9.18) [19].

## 2.5. Determination stoichiometry of the new metal chelates

Molar ratios and continuous variation [14–18] were used for estimation of equilibrium constant in solutions. Solutions of the DAPH ligand and metal salts were stirred, then allowed to equilibrate. Absorbance was recorded at individual λ<sub>max</sub> of each compound. An aliquot of 10 mL of stock solutions was diluted in 10 different-sized volumetric

flasks to prepare concentrations for further testing. The initial concentration of metal ions and imine ligands was 10 mM, following the method reported in the previous work [19].

## 2.6. Calculations of the apparent formation constants of the new metal imine chelates

Formation constants ( $K_f$ ) for the new chelates were obtained, as shown in Equation (S1) in Supporting Data using spectrophotometric methods [14–18]. The free energy change ( $\Delta(G^*)$ ) of the chelates is given by  $\Delta(G^*) = -RT \ln K_f$  at 25 °C.  $K_f$  is the formation constant, where  $T$  is the temperature in Kelvin and  $R$  is the universal gas constant.

## 2.7. Kinetic parameters

Kinetic parameters associated with decomposition of the complexes were obtained using the Coats–Redfern equation [17]. Thermodynamic parameters, such as the activation energy ( $E^*$ ), entropy activation ( $\Delta S^*$ ), enthalpy ( $\Delta H^*$ ), and Gibbs free energy change ( $\Delta G^*$ ) were calculated using Equation (S2) in the Supporting Data. A straight line was obtained by plotting the left-hand side of Equation (S2) versus  $1/T$ . The slope of the line is  $E^*$  and, from the intercept,  $A$  was calculated. We obtained the kinetic activation parameters such as entropy ( $\Delta S^*$ ), enthalpy ( $\Delta H^*$ ), and free energy of activation ( $\Delta G^*$ ) from Equations (S3)–(S5) in the Supporting Data [14–17].

## 2.8. Biological activity

We tested the biocidal screening of the new DAPH imine ligand and its metal chelates versus different strains of bacteria (*Serratia marcescens* (–ve), *Escherichia coli* (–ve), and *Micrococcus luteus* (+ve)) through using nutrient agar as a suitable diffusion method [14–20]. The antifungal activity of the investigated compounds was also evaluated, using the diffusion method against certain strains of fungi (*Aspergillus flavus*, *Geotrichum candidum*, and *Fusarium oxysporum*) with potato dextrose agar (PDA) as a circumference as mentioned before in detail in our previous work [14–20].

## 2.9. DNA Binding

ACT-DNA stock solution was prepared by mixing 50 mM NaCl and 5 mM Tris-HCl in distilled water at pH 7.5. The concentration of CT-DNA was estimated using the extinction coefficient of CT-DNA at 260 nm ( $6600 \text{ M}^{-1} \text{ cm}^{-1}$ ). The absorption ratio at 260 and 280 nm was 1.9:1, implying that the DNA solution contained no protein [14–17]. The stock solution was stored at 4 °C and used up to 4 d. EB concentration at 480 nm ( $\epsilon = 5860 \text{ M}^{-1} \text{ cm}^{-1}$ ) was estimated. Chelate solutions were prepared by dissolving a calculated amount of PdDAPH, AgDAPH, and VODAPH in 4% DMSO/Tris buffer, pH 7.5.

### 2.9.1. *Uv-visible absorption titration*

The interaction of metal complexes with CT-DNA was investigated using UV-vis absorption titration carried out using constant concentration of the metal complexes, while varying the DNA concentrations. Absorption of free CT-DNA was controlled with equimolar CT-DNA in buffer. Spectra thus likely resulted from DNA-metal chelate and the metal chelate aggregations [14–20]. We developed an intrinsic binding invariable ( $K_b$ ) by plotting  $[DNA]/(\varepsilon_a - \varepsilon_f)$  versus  $[DNA]$  as in Equation (S6) in the Supporting Data. In particular,  $\varepsilon_f$  was obtained from calibration curves for the new metal chelates.  $\varepsilon_a$  was evaluated using Beer's Law as the proportion between the M(II) chelate concentration and absorbance,  $A_{obs}$ , of metal chelate. Input data from Equation (S6) are acceptable with a slope equivalent to  $1/(\varepsilon_b - \varepsilon_f)$ , a y-intercept equivalent to  $1/(K_b(\varepsilon_b - \varepsilon_f))$ , and  $K_b$  as slope/intercept. DNA-binding for standard free energy was evaluated with the expression in Equation (S7) [14–20].

### 2.9.2. *Hydrodynamic assessments*

Hydrodynamic estimations used an Oswald miniaturized scale viscometer. Solutions were allowed to equilibrate at a constant temperature of 25 °C, as discussed in our previous work [16, 19].

### 2.9.3. *Agarose gel electrophoresis*

Agarose gel electrophoresis was used to examine DNA-binding products as thoroughly discussed in our previous work [15, 17].

## 2.10. *Cytotoxic studies*

Anticancer activity assays were performed at the Cancer Biology Department, National Cancer Institute, Cairo University, and Pharmacology Department. Optical density (OD) was assessed mainly spectrophotometrically at 564 nm with an ELISA microplate reader (Meter tech.  $\Sigma$  960). Cytotoxic activity of the DAPH imine ligand and new metal chelates were evaluated against human carcinoma cells, including hepatic cancer (HepG-2), breast cancer (MCF-7), and human colon cancer (HCT-116) using sulfo-rhodamine-b staining (SRB) [14, 18–20]. Cells from target cell lines were placed in 96-multi-well plates ( $10^4$  cells/well) for 24 h at 37 °C in a 5% CO<sub>2</sub> atmosphere to allow cell attachment. A series of concentrations of new compounds (0, 1, 2.5, 5, and 10  $\mu$ M) was added to the wells and incubation continued for 48 h. Cells were then fixed, washed, and dyed with SRB [14, 18]. Acetic acid was used to remove excess stain, and staining was fixed in Tris EDTA buffer. An ELISA reader was utilized to measure color intensity. The absorption for wells was expressed as percentage of cell viability. The IC<sub>50</sub> values (concentration required to inhibit 50% of cell growth) were obtained from dose-response curves and compared to results obtained for a vinblastine standard [14, 18]. The relationship between the fraction of viable cells and compound concentration was plotted to generate survival curves for each cell line. The experiment was performed in triplicate. Percent inhibitory concentration (IC %) was calculated [14, 18–20] using Equation (S8).

### 3. Results and discussion

#### 3.1. Physicochemical properties of the DAPH and its complexes

##### 3.1.1. $^1\text{H}$ NMR and $^{13}\text{C}$ NMR spectra of DAPH ligand

Interaction of host–guest molecules DA and PH to afford the desired imine (DAPH) ligand was probed via  $^1\text{H}$  NMR and  $^{13}\text{C}$  NMR spectra. In this respect, the  $^1\text{H}$  NMR spectrum of DAPH exhibited two broad signals at  $\delta = 9.90$  and  $9.40$  ppm that refer to two protons of two  $-\text{NH}$  groups and a singlet signal at  $\delta = 2.44$  ppm assigned to methyl group protons. Furthermore, multiplet signals at  $8.00$ – $6.86$  ppm were observed, attributed to 13-CH aromatic protons (Figure S1).  $^{13}\text{C}$  NMR (Figure S2) displayed a signal at  $145.62$  ppm, consistent with the presence of two azomethine carbon atoms. The spectrum also shows a signal at  $112.00$  ppm that probably represents the two symmetrical methyl carbons, whereas signals in the region  $113.95$ – $129.46$  ppm are assigned to phenyl and pyridine carbons.

The  $^1\text{H}$  NMR spectrum of the AgDAPH complex (Figure S3) is consistent with the presence of framework protons for the DAPH molecule. The spectrum displays two broad signals at  $\delta = 9.81$  ppm and  $9.79$  ppm, assigned to two protons of  $-\text{NH}$  groups and a singlet signal at  $\delta = 2.43$  ppm attributed to the two methyl groups. Multiplet signals at  $8.01$ – $6.85$  ppm are indicative of the 13-CH aromatic protons.

Similarly,  $^1\text{H}$  NMR spectrum of the diamagnetic PdDAPH complex (Figure S4) shows a singlet signal at  $\delta = 3.45$  ppm; this signal could refer to two protons of  $\text{H}_2\text{O}$  molecule, whereas the singlet signal at  $\delta = 2.43$  ppm is assigned to protons of two methyl groups. Also, multiplet signals of 13-CH aromatic protons were found at  $8.01$ – $6.83$  ppm.

##### 3.1.2. Elemental analysis and electrical conductivity

At room temperature, all new complexes are stable solids, colored, and display decomposition temperatures above  $300^\circ\text{C}$ . Elemental analysis for the imine (DAPH) ligand and its complexes (M-DAPH) indicated that the ligand is tridentate and coordinates with Pd(II), V(IV)O, and Ag(I) in 1:1 molar ratios as illustrated in Scheme 1 and Table S1. Molar conductance measurements of PdDAPH, VODAPH, and AgDAPH in DMF and ambient temperature were  $16.63$ ,  $14.00$ , and  $10.93\ \Omega^{-1}\ \text{cm}^2\ \text{mol}^{-1}$ , respectively. These values confirm their non-electrolytic nature [14–18].

##### 3.1.3. Infrared spectra

The FT-IR spectra of free DAPH ligand and its corresponding V(IV)O complex are shown in Figures S5 and S6, respectively. Characteristic IR bands from  $-\text{CH}=\text{N}$  moieties were detected, which confirmed the proposed ligand structure and its bonding with metals, as presented in Table 1. Importantly, the strong band at  $1599\ \text{cm}^{-1}$  in DAPH ligand may be assigned to  $-\text{C}=\text{N}$  stretching vibration. This band undergoes a red-shift to  $1565$ – $1601\ \text{cm}^{-1}$  upon complexation, thereby reflecting the involvement of azomethine nitrogen atoms in the formation of the complexes [13, 18, 21]. This conclusion is further supported by the appearance of a new band at  $465$ – $486\ \text{cm}^{-1}$  that corresponds to stretching vibration of the M–N bond. The band at  $3388\ \text{cm}^{-1}$  was



**Table 1.** Characteristic IR bands of the prepared DAPH imine ligand and its complexes.

Compounds	$\nu(\text{OH})/\text{H}_2\text{O}$	$\nu(\text{CH})_{\text{ar.}}$	$\nu(\text{C}=\text{N})$ vs	$\nu_{\text{py.}}(\text{C}=\text{N})$	$\nu(\text{NH})$	$\nu(\text{M}-\text{N})_{\text{w}}$
DAPH	3388 (s)	3093	1599	1536	3265	–
PdDAPH	3427	3051	1597	1489	3344	483
VODAPH	3444	3054	1601	1451	3343	486
AgDAPH	3443	3053	1565	1497	3261	465

vs: very strong; s: strong; m: medium; w: weak; ar.: aromatic; ph.: phenolic; py.: pyridine

spotted on the ligand spectrum as a result of stretching vibrations of free  $\text{H}_2\text{O}$  molecules.

IR spectra for the VODAPH (Figure S6) displayed a band at  $990\text{ cm}^{-1}$  that may reflect  $\text{V(IV)O}$  vibration in monomeric complexes [15, 16]. Further, peaks at  $880\text{--}883\text{ cm}^{-1}$  are assigned to rocking mode due to water coordination in the complex [15, 16]. Importantly, IR spectra of all MDAPH (imine) complexes exhibit a broad band at  $3427\text{--}3444\text{ cm}^{-1}$ , which is attributed to stretching vibrations  $\nu(\text{OH})$  of hydrated water molecules. This finding is consistent with elemental analysis results shown in Table S1. The distinctive frequencies for the coordinating nitrate group in AgDAPH have three modes that are non-degenerated at  $1470\text{ cm}^{-1}$   $\nu(\text{NO}_2)_{\text{asr}}$ ,  $1356\text{ cm}^{-1}$   $\nu(\text{NO}_2)_{\text{sym}}$ , and  $858\text{ cm}^{-1}$   $\nu(\text{NO})$ .

### 3.1.4. Mass spectra

Mass spectra of both  $\text{V(IV)O}$  and Ag complexes (Figures S7 and S8) showed molecular ion  $[\text{M}]^+$  peaks as  $m/z = 424$  for VODAPH and  $m/z = 531$  for AgDAPH. These peaks are in excellent agreement with the calculated formula weights of the complexes. Additionally, Scheme S1 showed the successive fragmentation of VODAPH at  $m/z = 343, 265, 209, 166, 75$ , and  $57$ . These data fit nicely with the proposed molecular formula for this complex.

### 3.1.5. Electronic spectra

UV-vis ( $200\text{--}800\text{ nm}$ ,  $298\text{ K}$ ) absorption spectra (Figure S9) of the DAPH ligand and its complexes were recorded in DMF solutions. As depicted in Table S2, DAPH shows absorption band around  $400\text{ nm}$  that refers to  $n \rightarrow \pi^*$  transition that arises from the imine (azomethine) group [21–23], together with another band at  $290\text{ nm}$ , which is attributed to  $\pi \rightarrow \pi^*$  transition of the aromatic rings of DAPH ligand. In the case of the prepared metal complexes, absorption bands at  $\lambda_{\text{max}} = 290\text{--}360\text{ nm}$  were assigned  $n \rightarrow \pi^*$  transition of the imine group in the DAPH ligand in the complexes to charge-transfer from DAPH imine ligand to the metal ions (LMCT). These charge transfers may occur between p-orbitals of the imine ligand and the d-orbitals of metal ions. Notably, the appearance of a broad low-intensity band at higher wavelength in the range of  $360\text{--}478\text{ nm}$  ( $\epsilon_{\text{max}} = 590\text{--}1710\text{ M}^{-1}\text{ cm}^{-1}$ ) most likely is caused by charge-transfer from DAPH imine LMCT, as a result of  $\pi$  electron interactions between the metal and ligand [24–28].

### 3.1.6. Magnetic measurements

Magnetic susceptibility measurements offer insights into the geometric structure of the chelates. The magnetic moment plays an important role in identifying the geometry of coordination around the metal ion (Table S1). PdDAPH and AgDAPH do not

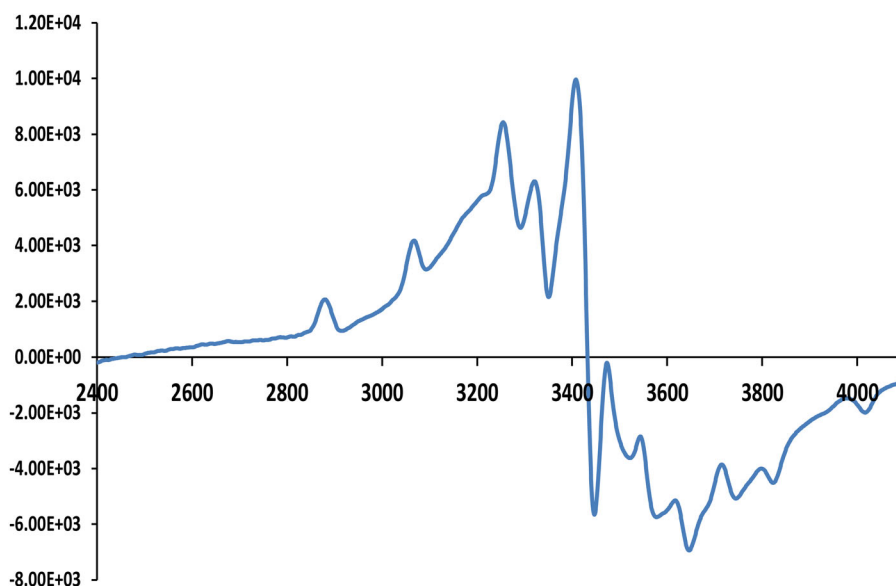


**Figure 1.** Electron paramagnetic resonance (EPR) spectra of VODAPH complex.

exhibit any magnetic moment, confirming that these complexes are diamagnetic having tetrahedral and square planar geometry, respectively [29, 30]. In contrast, VODAPH displays a magnetic moment of 1.87 BM, close to the spin-only magnetic moment for  $d^1$  and matches values for the distorted square pyramidal of V(IV)O [15].

### 3.1.7. EPR study

ESR spectrum shown in Figure 1 is quite diagnostic of  $d^1$  V in the +4 oxidation state and supports our proposed structure for V(IV)O in Scheme 1. The spectrum shows a hyperfine pattern of typical eight equidistant lines originating from the interaction of an unpaired electron with  $^{51}\text{V}$ ,  $I = 7/2$ . The  $A_{||}$  component of the  $^{51}\text{V}$  hyperfine splitting (hfs) should show eight lines, each separated by the same amount. Starting at low field, the first two lines are well resolved and separated by about 180 G. The total *spread* between the eight  $A_{||}$  lines should be about  $180 \times 8 = 1440$  G. This value indicates that an unpaired electron is present in the ( $d_{xy}$ ) orbital with a square pyramidal geometry around the oxido vanadium(IV) complex as reported for other related V(IV)O complexes [15].

### 3.1.8. Thermal gravimetric analysis

Thermal gravimetric analysis (TGA) of all prepared metal complexes was undertaken to probe their stability as a function of temperature along with the detection of water molecules, particularly the representative VODAPH complex as described in Scheme S1. Closer inspection of the obtained data for all M-DAPH complexes ( $M = \text{Ag}^+$ ,  $\text{Pd}^{2+}$ , and  $\text{V}^{4+}$ ) revealed loss of either hydrated  $\text{H}_2\text{O}$  as in the case of AgDAPH or coordinated water molecules, which occurred at much higher temperature (179 °C for VODAPH, 192 °C for PdDAPH) as proposed in Scheme S2. TGA data obtained for the three metal complexes can be summarized as follows: VODAPH showed decomposition up to 582 °C. First, one water molecule is lost before 179 °C; decomposition then

**Table 2.** Thermo-kinetic activation parameters of each decomposition step for the prepared complexes.

Complex	$E^*$ (KJmol <sup>-1</sup> )	A (S <sup>-1</sup> )	$\Delta H^*$ (KJmol <sup>-1</sup> )	$\Delta G^*$ (KJmol <sup>-1</sup> )	$\Delta S^*$ (Jmol <sup>-1</sup> K <sup>-1</sup> )
PdDAPH	17.40	0.16	16.50	44.99	-255.12
			15.20	82.80	-259.08
			14.20	115.20	-262.32
VODAPH	25.50	.063	24.60	52.10	-259.34
			23.30	93.80	-266.93
			21.60	147.60	-271.62
Residue			—	—	—
AgDAPH	17.10	.028	16.50	35.40	-262.87
			15.70	62.70	-270.21
			14.40	103.90	-275.40
			13.1	146.8	-278.64

occurs in two stages and exhibits mass loss of nearly 30.95% (calc. 30.99%), 49.06% (calc. 49.07%) over the temperature ranges of 181–347 °C and 349–582 °C, respectively. The residual after decomposition was V(IV)O.

As for AgDAPH complex, loss of hydrated water molecule (found 3.38%, calc. 3.39%) occurred within the temperature range of 33–110 °C, followed by another mass loss at a bit higher temperature range (112–237 °C), which is attributed to the removal of coordinated nitrate group. The third step showed a mass loss within the temperature range 239–410 °C (found 25.03%, calc. 25.05%) resulting from the removal of the C<sub>8</sub>H<sub>9</sub>N<sub>2</sub> part of the ligand. The final product was identified as (C<sub>13</sub>H<sub>12</sub>N<sub>3</sub>+Ag) [18].

PdDAPH displayed three degradation steps in the temperature range 34–650 °C. The first step was observed at 34–194 °C with a mass loss of 3.89% (calc. 3.87%), attributed to the loss of one coordinated water molecule. The second step was observed at 194–328 °C with a mass loss of 28.33% (calc. 28.36%), consistent with the removal of remaining part of the DAPH imine ligand (C<sub>8</sub>H<sub>8</sub>N<sub>2</sub>). The third stage was in the range 330–440 °C, with an estimated mass loss of 67.74% (calc. 67.77%). This mass could be attributed to loss of the remaining part of the complex (C<sub>13</sub>H<sub>11</sub>N<sub>3</sub>+Pd). Taken together, the combined TGA results of the three complexes nicely matched the suggested stoichiometry obtained from elemental analysis [15, 21, 22, 31].

### 3.1.9. Kinetic aspects

The kinetic parameters associated with degradation steps of the prepared M-DAPH complexes showed negative entropy changes ( $\Delta S^*$ ) as summarized in Table 2. These findings indicate that metal chelates are more ordered in their active state than parent reactants. Degradation reactions were endothermic, reflected in positive values of  $\Delta H$ . Large positive values for free energy activation ( $\Delta G^*$ ) indicates that degradation reactions are slower than formation for most steps in the degradation process. An obvious relationship exists between (A) and ( $E^*$ ). The slow pyrolysis reaction occurs at relatively low energy (A), and the larger positive value of ( $E^*$ ) demonstrates vibrational, rotational, and translational states, besides changes in mechanical energy [22].

### 3.1.10. Stoichiometry and formation constant of M-DAPH complexes

Two spectrophotometric methods, molar ratio, and continuous variations indicated a stoichiometry of 1:1 M:L of the chelates. Results from continuous variation analysis

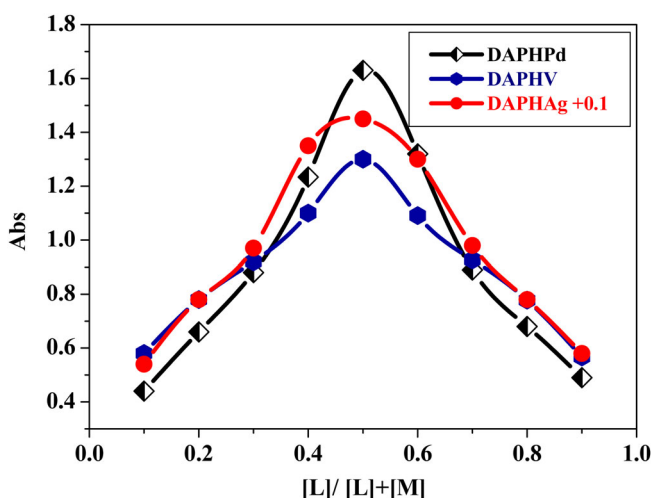


**Figure 2.** Continuous variation plots for the prepared complexes in aqueous-ethanolic medium at  $[PdDAPH] = [VODAPH] = [AgDAPH] = 10^{-3}$  M and 298 K.

**Table 3.** The formation constant ( $K_f$ ), stability constant (pK) and gibbs free energy ( $\Delta G^*$ ) values of the synthesized complexes at 298 K.

Complex	Type of complex	$K_f$	Log $K_f$	$\Delta G^*$ (kJmol $^{-1}$ )
PdDAPH	1:1	$2.58 \times 10^4$	4.41	−25.17
VODAPH	1:1	$7.28 \times 10^4$	4.86	−27.74
AgDAPH	1:1	$1.17 \times 10^4$	4.07	−23.21

display maximum absorbance at mole fractions of 0.5–0.6, indicating a 1:1 (ligand:metal) stoichiometry as evident from Figure 2. Results of molar ratio measurements confirmed this stoichiometry (Figure S10) [14–18].

Spectrophotometric measurements using continuous variation method (Table 3) were utilized to determine the formation constants ( $K_f$ ) of new metal chelates formed in solution. Calculations demonstrate that  $K_f$  values reflect the stability of the new chelates.  $K_f$  values for chelates decrease in the order  $VODAPH > PdDAPH > AgDAPH$ . We also calculated Gibbs free energy ( $\Delta G^\ddagger$ ) and the stability constant (pK). The spontaneous formation reaction occurred due to the negative  $\Delta G^\ddagger$  values. Substantial stability in the pH range of 4–9 was displayed by pH-profiles (absorbance versus pH) shown in Figure 3. This result demonstrates the ability of DAPH ligands to stabilize metal chelates. Consequently, suitable pH for desired applications of the new metal–imine complexes may extend from pH 3.5 to pH 11.

### 3.2. Biological properties of the complexes

A primary objective for the development of antimicrobial and anticancer agents is patient safety. Antibacterial activity of DAPH complexes was tested using various bacterial strains in order to increase the chance of detecting their antimicrobial properties. Thus, *in vitro* antimicrobial activities of DAPH ligand and its metal chelates were

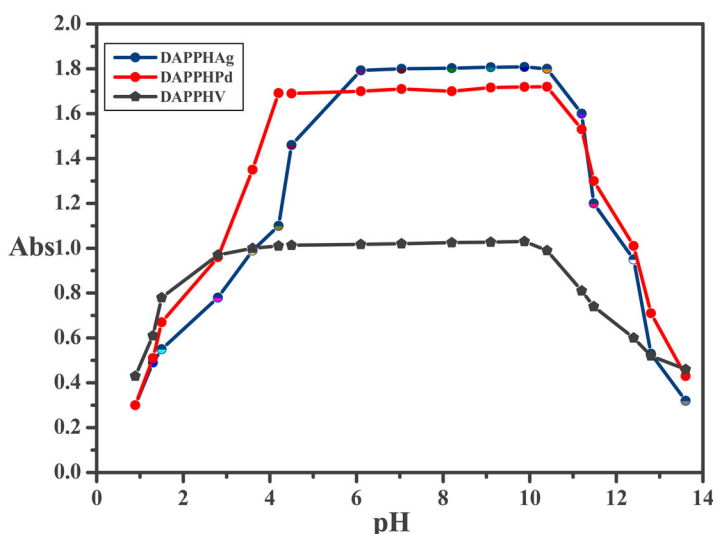


**Figure 3.** Dissociation curve of imine complexes in DMF.

evaluated against three different types of bacteria, *E. coli* (–ve), *S. marcescens* (–ve), and *luteus* (+ve) as well as three fungi, *A. flavus*, *G. candidum*, and *F. oxysporum* [14, 15, 23]. The obtained results are summarized in Table 4. Importantly, serial dilution method was used to determine the minimum inhibitory concentration (MIC) as depicted in Table 5. Generally, all tested metal complexes (M-DAPH) exhibited higher inhibitory influence than the free DAPH ligand or the metal precursors alone, as evident from Figures S11 and S12. This marked difference in antimicrobial activity can be accounted for by chelation theory, as seen with other conceptually and structurally related compounds [14]. In this respect, previous work suggested that chelation may increase the efficacy of ligands as bacteriostatic and bactericidal agents [23, 32], and our results are consistent with this conclusion. The fact that DAPHPd exhibited the highest toxicity and lowest MIC toward *E. coli* and *G. candidum*, respectively (1.25 and 2.25  $\mu\text{g/mL}$ ), it raised the concern about the identity of metal ion in the designed. Since all prepared complexes contain the same DAPH ligand, this massive discrepancy in activity is likely to be caused by metal ion. As previously reported the metal ion increases activity through alterations in a number of important parameters such as solubility, dipole moment, conductivity, and cell permeability [13–17].

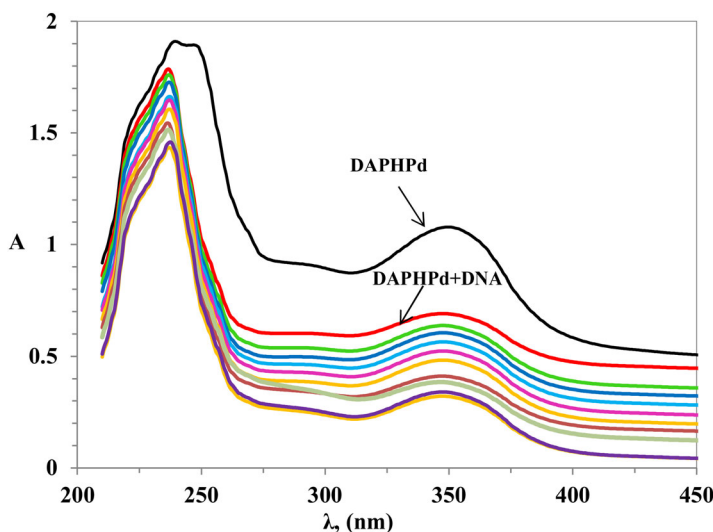
Table 5 provides a comparison of the antibacterial activity (MIC) of our M-DAPH compounds with structurally closely related M-HNAP analogues (M = Pd, V, and Ag) against *E. coli*, *S. marcescens*, and *M. luteus*. It is clearly evident that our compounds gave lower values of MIC, implying a more effective antimicrobial inhibitor [18]. The same trend was also established regarding the antifungal activity as depicted in Table 5. The enhanced antimicrobial activity observed for the M-DAPH complexes could be explained in terms of different geometric structure/composition of the imine ligand as well as the type and number of coordination sites. These parameters are expected to have strong impact on dipole moment, conductivity, and cell permeability of the different pathogens.

**Table 4.** Results of antimicrobial of the prepared DAPH ligand and its metal complexes against different strains of bacteria and fungi.

Compounds	± SDinhibition zone (mm)											
	<i>Escherichia coli</i> (–ve)		<i>Serratia marcescens</i> (–ve)		<i>Micrococcus luteus</i> (+ve)		<i>Fusarium oxysporum</i>		<i>Getrichm candidum</i>		<i>Aspergillus flavus</i>	
Conc. (mg/mL)	10	20	10	20	10	20	10	20	10	20	10	20
DAPH	5 ± 0.05	8 ± 0.03	9 ± 0.12	13 ± 0.19	11 ± 0.14	16 ± 0.14	7 ± 0.08	11 ± 0.05	9 ± 0.03	13 ± 0.07	6 ± 0.05	9 ± 0.10
PDAPH	±0.1313	23 ± 0.12	17 ± 0.10	±0.0529	23 ± 0.11	40 ± 0.26	19 ± 0.16	30 ± 0.11	22 ± 0.05	38 ± 0.15	12 ± 0.06	24 ± 0.12
VODAPH	±0.0710	±0.0919	14 ± 0.11	25 ± 0.18	19 ± 0.17	36 ± 0.08	16 ± 0.14	27 ± 0.12	20 ± 0.07	35 ± 0.17	10 ± 0.04	21 ± 0.06
AgDAPH	11 ± 0.12	21 ± 0.11	15 ± 0.12	27 ± 0.11	22 ± 0.05	39 ± 0.19	17 ± 0.13	28 ± 0.19	21 ± 0.06	36 ± 0.13	11 ± 0.03	23 ± 0.10
Ofloxacin												
Fluconazole	14 ± 0.05	24 ± 0.19	18 ± 0.10	29 ± 0.25	24 ± 0.18	41 ± 0.32	19 ± 0.11	30 ± 0.15	23 ± 0.24	39 ± 0.26	13 ± 0.10	24 ± 0.17

**Table 5.** Minimum inhibition concentration (MIC) for antimicrobial assay of the prepared imine and its complexes.

Compounds	Bacteria			Fungi		
	<i>E. coli</i>	<i>M. luteus</i>	<i>S. marcescens</i>	<i>A. flavus</i>	<i>G. candidum</i>	<i>F. oxysporum</i>
DAPH	3.25	4.00	4.75	4.75	4.25	4.50
PdDAPH	1.25	1.75	2.00	2.75	2.25	2.50
VODAPH	1.75	2.50	3.00	3.50	3.00	3.25
AgDAPH	1.50	2.25	2.50	3.00	2.50	2.75
Ofloxacin	1.25	1.75	0.85			
Fluconazole				2.00	1.75	2.50

**Figure 4.** Spectral scans of interactions of the PdDAPH complex ( $10^{-3}$  M) in 0.01 M Tris buffer (pH 7.2, 298 K) with CT-DNA (0–30)  $\mu$ M DNA, from top to bottom.

### 3.3. DNA binding assay

#### 3.3.1. Electronic spectra of DNA interactions

Spectrophotometric titration is an important method for investigating the mode of binding for CT-DNA and metal chelates. Spectra were recorded by gradually adding buffer of pre-treated CT-DNA to buffer solutions of chelates as illustrated in Figure 4. Intercalation typically occurs when intercalated ligand orbitals are linked to orbital base pairs  $-\pi-\pi^*$ ; transition energy is reduced and leads to bathochromic shift. When a conjugation orbital is half-filled with electrons, it minimizes the transition probabilities and leads to a hypochromic shift [14].

The electronic absorption spectrum for PdDAPH (Figure 4) in the presence and absence of several buffered CT-DNA concentrations indicates that increasing the amount of CT-DNA causes a decrease in absorbance of the metal chelate. Binding constants ( $K_b$ ) and spectral parameters for DNA interaction were calculated using Equation (S6); the extracted data are graphically presented in Figure S13 and summarized in Table 6 [32]. In view of these results, it can be concluded that binding modes

**Table 6.** Spectral parameters for the interaction of the prepared imine complexes.

Complex	$\lambda_{\text{max}}$ free (nm)	$\lambda_{\text{max}}$ bound (nm)	$\Delta n$	Chromism (%) <sup>a</sup>	Type of chromism	Binding constant $10^4$ ( $K_b$ ) <sup>b</sup>	$\Delta G^*$ (KJmol <sup>-1</sup> )
DAPH	368	356	12	19.00	Hypo	1.04	−22.18
	251	240	11	14.00	Hypo		
PdDAPH	349	351	2	36.84	Hypo	6.02	−27.27
	247	236	11	6.44	Hypo		
VODAPH	369	351	18	23.81	Hypo	4.27	−26.42
	290	276	14	21.13	Hypo		
	252	239	13	16.75	Hyper		
AgDAPH	363	354	9	40.85	Hypo	2.87	−25.43
	252	238	14	18.62	Hyper		

<sup>a</sup>Chromism (%) =  $(\text{Abs}_{\text{free}} - \text{Abs}_{\text{bound}})/\text{Abs}_{\text{free}}$  (Liu et al., 2008; Abdel-Rahman et al., 2015 a, b; Abdel-Rahman et al., 2016 a, b).

<sup>b</sup>Binding constant  $K_b = \text{M}^{-1}$ .

of the DAPH ligand and its complexes with CT-DNA could occur *via* both alternative and intercalative modes in the order PdDAPH > VODAPH > AgDAPH > DAPH.

### 3.3.2. Measurements of viscosity

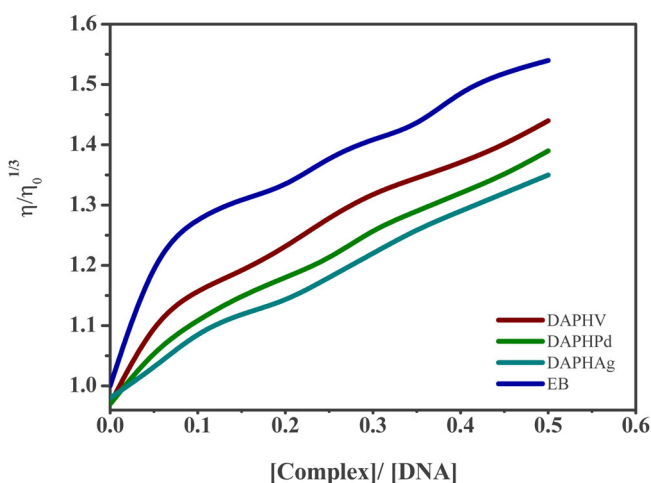
Viscosity measurements were also employed to explore interaction modes between the metal complexes and CT-DNA. Hydrodynamic viscosity measurements are sensitive to length changes of DNA and are an efficient method for investigating DNA-binding mode for new compounds. In this respect, viscosity measurements were undertaken in the presence of EB, a well-known and standard reagent that binds to base pairs in DNA, thereby causing an increase in DNA viscosity. The length of DNA is not affected by electrostatic binding, resulting in a constant viscosity of DNA [18, 32, 33]. Therefore, the above results indicate that partial intercalation by complexes into the DNA helix leads to a decrease in effective length and increased viscosity [14, 34–36].

Figure 5 demonstrated that the solution of DNA's relative viscosity clearly enhances when the quantity of the metal-imine chelate rises. That could be the effect of the aromatic moiety in the DAPH ligand in the base pairs of DNA that causes a crook in the DNA helix, an increase in the base pairs segregation on the intercalation site, and consequently an increment of the DNA molecular length [15].

### 3.3.3. Gel electrophoresis

DNA binding of the prepared M-DAPH complexes was examined using agarose gel electrophoresis as shown in Figure 6. Gels showed intense bands for all DNA samples, thereby indicating efficient binding to DNA by all M-DAPH chelates (M = Pd(II), V(IV)O, and Ag(I)). Variation in banding patterns was clear between samples treated with metal-imine chelates compared to control DNA. No cleavage was observed in control DNA; metal chelates (M-DAPH) apparently caused such cleavage [18, 35]. Although mechanistic aspects of DNA cleavage by metal chelates are ambiguous, the obtained results implied that identity of metal ions plays a vital role in the interaction with DNA [15, 36]. Thus, it is concluded that M-DAPH chelates may inhibit the growth of the pathogenic organisms through interactions with the genome.





**Figure 5.** The effect of increasing concentration of complexes on relative viscosity of DNA, [DNA] = 0.5 mM, [complex] and [EB] = 25–250  $\mu$ M and 298 K.

### 3.3.4. Suggested mechanisms for complexes-DNA-interactions

Correlation among spectroscopic, hydrodynamic measurements, and DNA binding are consistent with several binding modes. Generally, metal chelates bind with DNA mainly by hydrophobic or electrostatic interactions. The mechanism of interaction of CT-DNA with the representative complex, AgDAPH, might be regarded as follows: first, the negatively charged nitrate group may be replaced by H<sub>2</sub>O molecules in solution [14–18, 37]. Thus, the complex will carry a positive charge at the silver atom as a result of this displacement. Second, the negatively charged backbone in the phosphate group could attract the positive charge on a complex ion at the periphery of the double helix through electrostatic interaction. Finally, removing the nitrate ligand from the complex in solution may cause the complex to reconfigure with a planar area in the center. In view of these scenarios, possible interaction pathways for DNA with AgDAPH are shown in Scheme 2a and b. In principle, the first step involves interaction of the Ag(I) complex with the base backbone of DNA or an electrostatic interaction of the coordination sphere with base pairs of DNA. The second step occurs *via* inserting the planar area of the complex between DNA base pairs or coordination of Ag<sup>+</sup> with base pairs.

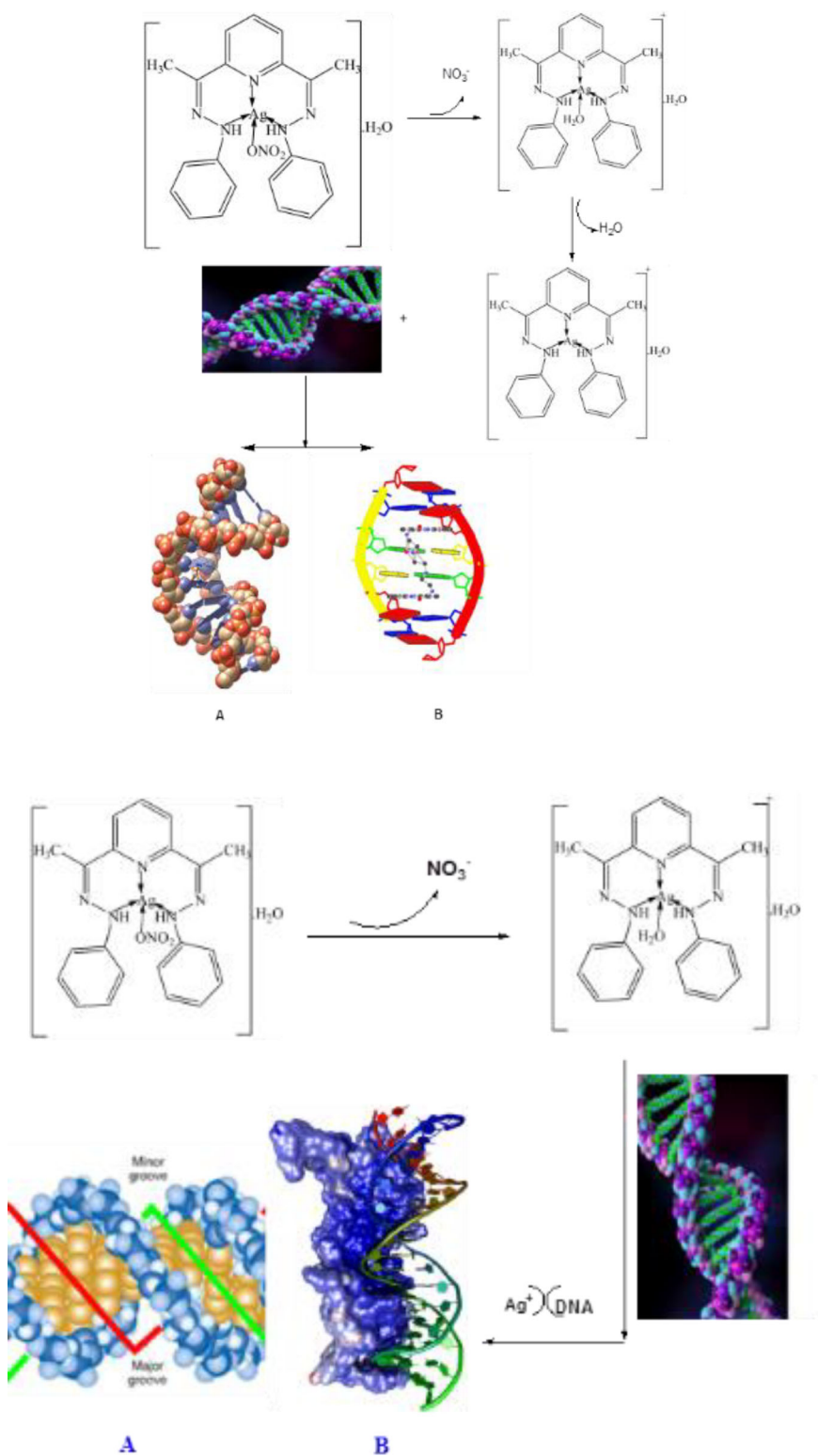
### 3.4. Antiproliferative activity

The cytotoxicity of new DAPH ligand and metal chelates were assessed using different human carcinoma cell lines, colon (HCT-116), hepatic (HepG-2), and breast (MCF-7), within a 0–10  $\mu$ M concentration range. Estimated IC<sub>50</sub> values demonstrated that metal chelates mostly display higher cytotoxicity than that of the free ligand and very close to IC<sub>50</sub> of vinblastine that was used as a positive control (see Table 7). The noted cytotoxic potency of the metal complexes could be linked to identity of the central metal atom, as suggested by Tweedy's chelation concept [37–39]. Estimated IC<sub>50</sub> values of 14.00–19.60  $\mu$ g/ $\mu$ L were obtained for HCT-116 cancer cells, whereas values were



**Figure 6.** DNA binding results of imine complexes based on gel electrophoresis. Lane 1: DNA ladder, lane 2: VODAPH + DNA, lane 3: AgDAPH + DNA, lane 4: PdDAPH + DNA.

6.50–12.40  $\mu\text{g}/\mu\text{L}$  in the case of HepG-2 and 9.50–18.90  $\mu\text{g}/\mu\text{L}$  for MCF-7 cancer cells. Cancer cell responses decrease in the order HepG-2 > MCF-7 > HCT-116. Highest cytotoxicity was associated with the PdDAPH complex on HepG-2 cancer cells with an  $\text{IC}_{50}$  value of 6.50  $\mu\text{g}/\mu\text{L}$ , followed by AgDAPH complex with an  $\text{IC}_{50}$  value of 9.50  $\mu\text{g}/\mu\text{L}$  and the VODAPH complex with an  $\text{IC}_{50}$  value of 12.40  $\mu\text{g}/\mu\text{L}$ . As reported on related work, the free DAPH ligand is less potent than all M-DAPH chelates [14, 38]. Gaetke and Chow mentioned that the presence of metal ions smooths the oxidative tissue that causes damage to DNA [15, 40, 41]. More importantly, the anticancer potency of the M-DAPH compounds was compared with previously reported metal complexes containing V(IV), Pd(II), and Ag (I) complexes [15, 18, 39], and the results are summarized in Table 8. It is evident that the  $\text{IC}_{50}$  values of our new compounds against HCT-116, HepG-2, and MCF-7 are lower than values reported for structurally similar compounds of different Schiff bases, thereby meaning more efficient anticancer agent. This implies that the structure of the new  $\text{N}_3$ -Schiff base ligand helped in enhancing the reactivity of the prepared metal complexes.



**Scheme 2.** (a) A suggested mechanism for interaction of AgDAPH with CT-DNA *via* (A) intercalation binding and (B) replacement (b) A suggested mechanism for interaction of AgDAPH with CT-DNA *via* groove binding (electrostatic and hydrogen bonding).

**Table 7.** Cytotoxic activity ( $IC_{50}$ ) of DAPH imine ligand and its complexes against Colon carcinoma cells (HCT-116 cell line), hepatic cellular carcinoma cells (HepG-2), and breast cancer cell lines (MCF-7).

Compounds	$IC_{50}$ ( $\mu\text{g}/\mu\text{L}$ )		
	HepG-2	HCT-116	MCF-7
DAPH	$105.00 \pm 0.06$	$156.00 \pm 0.07$	$98.00 \pm 0.11$
PdDAHP	$6.50 \pm 0.09$	$14.00 \pm 0.05$	$9.50 \pm 0.09$
AgDAHP	$9.50 \pm 0.07$	$16.60 \pm 0.10$	$11.30 \pm 0.10$
VODAPH	$12.40 \pm 0.08$	$19.60 \pm 0.06$	$18.90 \pm 0.04$

**Table 8.** Cytotoxic activity ( $IC_{50}$ ) of DAPH imine ligand and its complexes against Colon carcinoma cells (HCT-116 cell line), hepatic cellular carcinoma cells (HepG-2), and breast cancer cell lines (MCF-7) compared to previously reported similar compounds.

Compounds	$IC_{50}$ ( $\mu\text{g}/\mu\text{L}$ )			Reference
	HepG-2	HCT-116	MCF-7	
PdDAHP	$6.50 \pm 0.09$	$14.00 \pm 0.05$	$9.50 \pm 0.09$	This work
PdHNA	$12.30 \pm 0.11$	$20.0 \pm 0.09$	$14.50 \pm 0.04$	[18]
PdL	$30.50 \pm 0.13$	$38.40 \pm 0.05$	$26.80 \pm 0.07$	[39]
AgDAHP	$9.50 \pm 0.07$	$16.60 \pm 0.10$	$11.30 \pm 0.10$	This work
AgHNA	$14.10 \pm 0.10$	$22.45 \pm 0.05$	$14.10 \pm 0.09$	[18]
AgL	$35.2 \pm 0.06$	$39.50 \pm 0.09$	$31.00 \pm 0.06$	[39]
VODAPH	$12.40 \pm 0.08$	$19.60 \pm 0.06$	$18.90 \pm 0.04$	This work
VOHNA	$19.30 \pm 0.18$	$25.40 \pm 0.10$	$14.00 \pm 0.11$	[15]
VOHNA	$16.30 \pm 0.14$	$25.0 \pm 0.04$	$22.30 \pm 0.13$	[18]

**Table 9.** Antioxidant activity of DAPH imine ligand and its Pd, Ag and VO complexes towards the scavenging of DPPH radical compared to ascorbic acid.

Compounds	$IC_{50}$ ( $\mu\text{g}/\mu\text{L}$ )
DAPH	$62 \pm 0.10$
PdDAHP	$16 \pm 0.09$
AgDAHP	$21 \pm 0.08$
VODAPH	$24 \pm 0.12$
Ascorbic acid	$58 \pm 0.07$

### 3.5. Antioxidant activities of DAPH using DPPH radical scavenging

Antioxidants can show protective activity against cancer cells by decreasing oxidative stress that can cause damage to cells during metabolism. In this respect, free radicals play a significant role in pathogenic processes for many human diseases [42]. DPPH has been widely employed as a free radical scavenging assessment, owing to its ease of use. Antioxidant activity of the DAPH imine ligand and its M-DAHP complexes was evaluated *in vitro*, utilizing the DPPH free radical scavenging assay. Antioxidant potency at different concentrations (10, 25, 50, 100, and 150  $\mu\text{g}/\text{mL}$ ) was estimated and ascorbic acid was used as a positive control. The ligand showed moderate antioxidant activity, whereas metal complexes exhibited much greater antioxidant activity than the ligand. Notably, for all the complexes, the antioxidant activity increased with concentration. In this context, the DAPHV complex exhibited the least antioxidant activity, with  $IC_{50}$  of 75  $\mu\text{g}/\text{mL}$ , while the PdDAHP congener showed the highest antioxidant activity, with an  $IC_{50}$  of 16  $\mu\text{g}/\text{mL}$  as depicted in Table 9.

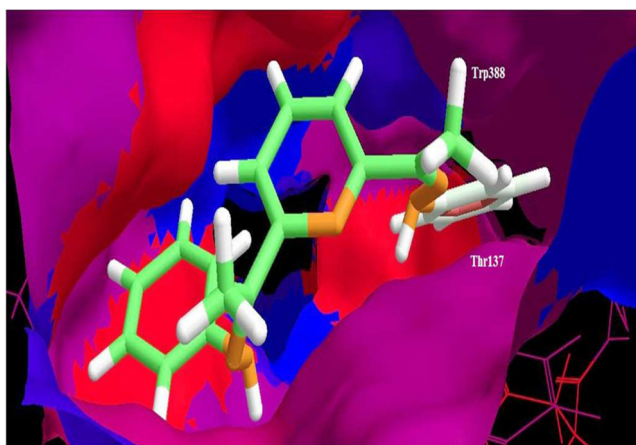


**Figure 7.** Surface representation of the hydrophobic binding model of DAPH with hydrophobic residues of GLUT1.

### 3.6. Molecular docking study

A rational approach in medicinal chemistry is analyzing three-dimensional structures for target proteins, which is considered an essential tool for the design and discovery of new targets. Docking data analyses indicated conformational changes at binding sites for amino acid residues. Optimized molecular structures for the DAPH ligand as well as Pd and Ag complexes, obtained from PM6 estimation, were used as an input file for a conformational search. The conformer with the lowest energy was used for the docking study.

We started the study by examining known structures taken from the protein data bank (PDB code 4PYP with resolution 3.70 Å), a single global archive for examining known structures. The desired ligand observed within the crystal structure of the enzyme is [2R,3S,4S,5R, 6R]-2-(hydroxyl methyl)-6-nonoxy-oxane-3,4,5-triol]. The ligand was removed from the binding pocket and subjected again to re-docking to characterize the GLUT1 active site (the grid dimensions were  $x = 583.93$ ,  $y = -29.39$ , and  $z = 200.08$  Å, and the radius is 15 Å). The root mean square deviation (RMSD) between the predicted and observed X-ray crystallographic conformers that can induce antitumor cell activity is 1.40 Å.

DAPH docking calculations using the target enzyme demonstrated van der Waals forces and hydrogen bonds as major interactions. As shown in Figure S20, DAPH displays two H-bond interactions with active site residues Gly 384 and Trp 388 with bond lengths of 2.24 and 3.47 Å, respectively. Thus, DAPH could act as an efficient antitumor drug for HepG2 cell lines as it contains hydrophobic phenyl and methyl moieties that are essential for the interaction with the lipophilic pocket of GLUT1. Moreover, the interaction of the DAPH with the binding pocket of GLUT1 displayed two hydrophobic interactions with residues Trp 388 and Phe 137, with distances of 3.247 and 2.899 Å, respectively. These interactions determine the stability of the drug-protein complex. A surface representation of the minimum energy structure of the GLUT1 and DAPH complex is provided in Figure 7.

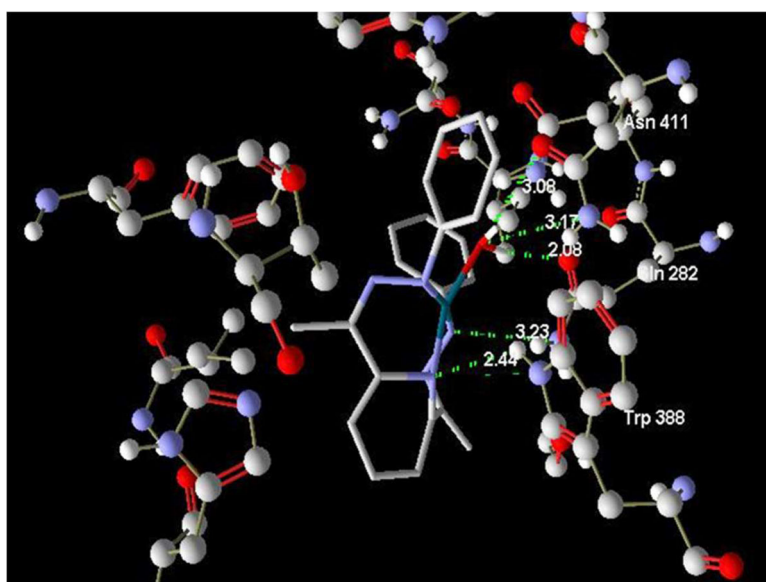


**Figure 8.** The hydrogen bond interactions of DAPHPd complex and the target protein.

### 3.6.1. The molecular docking analysis of PdDAPH complex

The PdDAPH complex fits deeply inside the active pocket of the enzyme, forming five hydrogen bonds and hydrophobic interactions, which suggest high stability and affinity. Hydrogen bonding was observed with residues Trp388 (2.44 Å), Gln282 (2.08 and 3.23 Å), and Asn411 (3.08 and 3.17 Å), as presented in [Figure 8](#). Hydrophobic interactions were found with Phe26 and Tyr 137 at distances of 2.80 and 1.57 Å, and the most stable docked pose for the surface representation of Pd-complex and GLUT1 enzyme is exhibited in [Figures 8](#) and S21. These interactions would enhance the inhibitory potency of the complex.

### 3.6.2. The molecular docking analysis of AgDAPH complex

As illustrated in [Figure 9](#), the oxygen and nitrogen atoms of the nitro group settle into two hydrogen bond interactions with Trp388 and Gln282 residues. All hydrogen bond lengths were found in the range of 2.14–3.56 Å. Practically, these interactions may contribute to the  $IC_{50}$  shown for the Ag-complex. Moreover, the high affinity of the Ag-complex could be explained in terms of the lipophilic interaction among hydrophobic amino acid residues and the methyl/phenyl moieties. The Trp137 and Ile 164 have distances of 2.51 and 2.48 Å, respectively. The surface representation of the most stable conformer is provided in [Figure S22](#).

## 4. Conclusion

Several aspects of coordination chemistry and biological activity imply that cytotoxicity of metal complexes comprising an aromatic moiety may be associated with various mechanisms of action. In this study, metal (V(IV)O, Pd(II), and Ag(I)) imine (DAPH)

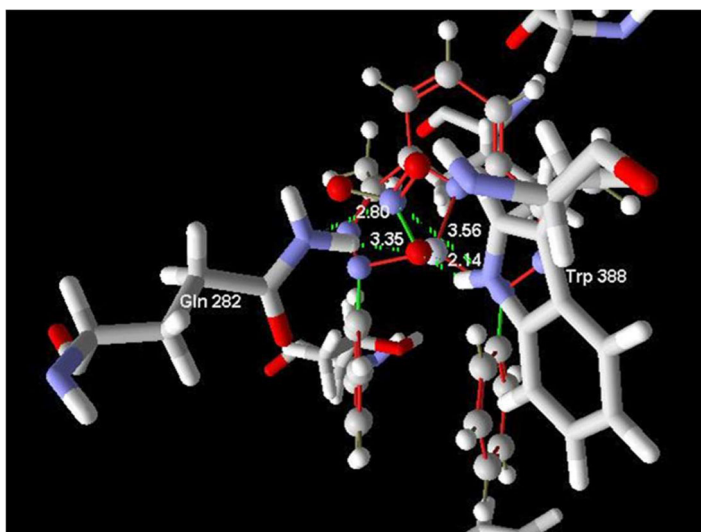


**Figure 9.** The hydrogen bond interactions of DAPHAg complex and the target protein.

chelates were specifically chosen because of their potential as drug candidates compared with other transition metal compounds. Thus, M-DAPH was successfully prepared and fully characterized, together with their biological activities and DNA-interactions. The combined results revealed that DAPH (imine) ligand acts as a tridentate NNN-ligand and coordinates with V(IV)O, Pd(II), and Ag(I) in 1:1 molar ratios. Complex geometries are tetrahedral for Ag(I), square planar for Pd(II), and distorted square pyramidal for V(IV)O. The M-DAPH/DNA interactions are consistent with intercalative, electrostatic, and replacement interaction modes. Importantly, antipathogenic screening showed that these metal chelates are ideal antimicrobial agents for various microbes. Growth inhibitory effects for suggested compounds was assessed using HCT-116, MCF-7, and HepG-2 cancer cell lines, with PdDAPH being the most efficient anticancer agent. Finally, docking studies showed that PdDAPH fit perfectly into the active site pocket of the GLUT1 enzyme, forming five hydrogen bonds and hydrophobic interactions.

### Acknowledgement

We extend our sincere appreciation to Researchers Supporting Project number (RSP-2020/79), at King Saud University, Riyadh, Saudi Arabia for funding this work.

### Disclosure statement

The authors declare no conflict of interest.

### Funding

Researchers Supporting Project (RSP-2020/79) at King Saud University, Riyadh, Saudi Arabia.



## References

- [1] C. Qian, C. Zhu, T. Huang. *J. Chem. Soc. Perkin Trans. 1.*, **114**, 2131 (1998).
- [2] L.H. Abdel-Rahman, A.M. Abu-Dief, M.O. Aboelez, A.A.H. Abdel-Mawgoud. *J. Photochem. Photobiol. B.*, **170**, 271 (2017).
- [3] B. Jeżowska-Trzebiatowska, P. Chmielewski, A. Vogt. *Inorg. Chim. Acta*, **83**, 129 (1984).
- [4] R.J. Motekaitis, A.E. Martell, D.A. Nelson. *Inorg. Chem.*, **23**, 275 (1984).
- [5] S.M. Abuo-el-Wafa, F.M. Ashmawy, R.M. Issa, C.A. McAuliffe, R.V. Parish. *Inorg. Chim. Acta*, **96**, 257 (1985).
- [6] S.C. Bhatia, J.M. Bindlish, A.R. Saini, P.C. Jain. *J. Chem. Soc. Dalton Trans.*, **17**, 737 (1981).
- [7] M.M.A. Mohamed, M.M. Shoukry. *Polyhedron*, **20**, 343 (2001).
- [8] J. Fuentes, R. Reboso, A. Rodriguez. *Polyhedron*, **8**, 2693(1989).
- [9] M.E. Bhowon. *J. Indian Chem. A*, **39**, 120 (2000).
- [10] D. Granchi, G. Ciapetti, L. Savarino, D. Cavedagna, M.E. Donati, A. Pizzoferrato. *J. Biomed. Mater. Res.*, **31**, 183 (1996).
- [11] R.C. Bray, G.N. George. *Biochem. Soc. Trans.*, **13**, 560 (1985).
- [12] R.V. Singh, S.C.S. Jadon, N. Gupta. *React. Inorg. Met. Org. Chem.*, **27**, 759 (1997).
- [13] I. Correia, S. Roy, C.P. Matos, S. Borovic, N. Butenko, I. Cavaco, F. Marques, J. Lorenzo, A. Rodríguez, V. Moreno, J.C. Pessoa. *J. Inorg. Biochem.*, **147**, 134 (2015).
- [14] L.H. Abdel-Rahman, A.M. Abu-Dief, R.M. El-Khatib, S.M. Abdel-Fatah. *J. Photochem. Photobiol. B.*, **162**, 298 (2016).
- [15] L.H. Abdel-Rahman, A.M. Abu-Dief, M. Basha, A.A.H. Abdel-Mawgoud. *Appl. Organomet. Chem.*, **31**, e3750 (2017).
- [16] L.H. Abdel-Rahman, A.M. Abu-Dief, M. Ismael, M.A.A. Mohamed, N.A. Hashem. *J. Mol. Struct.*, **1103**, 232 (2016).
- [17] L.H. Abdel-Rahman, A.M. Abu-Dief, E.F. Newair, S.K. Hamdan. *J. Photochem. Photobiol. B.*, **160**, 18 (2016).
- [18] L.H. Abdel-Rahman, A.M. Abu-Dief, M.R. Shehata, F.M. Atlam, A.A.H. Abdel-Mawgoud. *Appl. Organometal. Chem.*, **33**, e4699 (2019).
- [19] M.I. Hossain, M. Świtalska, W. Peng, M. Takashima, N. Wang, M. Kaiser, J. Wietrzyk, S. Dan, T. Yamori, T. Inokuchi. *Eur. J. Med. Chem.*, **69**, 294 (2013).
- [20] L.H. Abdel-Rahman, A.M. Abu-Dief, M.S. Adam, S.K. Hamdan. *Catal. Lett.*, **146**, 1373 (2016).
- [24] S. Chandra, S. Raizada, M. Tyagi, P. Sharma. *Spectrochim. Acta A Mol. Biomol. Spectrosc.*, **69**, 816 (2008).
- [21] E.M.M. Ibrahim, L.H. Abdel-Rahman, A.M. Abu-Dief, A. Elshafaie, S.K. Hamdan, A.M. Ahmed. *Phys. Scr.*, **93**, 05801 (2018).
- [22] M. Montazerzohori, S. Mojahedi Jahromi, A. Masoudiasl, P. McArdle. *Spectrochim. Acta, Part A*, **138**, 517 (2015).
- [23] L.P. Nitha, R. Aswathy, N.E. Mathews, N.E. Mathews, B.S. Kumara, K. Mohanan. *Spectrochim. Acta A Mol. Biomol. Spectrosc.*, **118**, 154 (2014).
- [25] A.A.A. Emara. *Spectrochim. Acta A Mol. Biomol. Spectrosc.*, **77**, 117 (2010).
- [26] M. Gaber, H. El-Ghamry, F. Atlam, S. Fathalla. *Spectrochim. Acta A Mol. Biomol. Spectrosc.*, **137**, 919 (2015).
- [27] W. Al Zoubi, A.A.S. Al-Hamdani, Y.G. Ko. *Sep. Sci. Technol.*, **52**, 1052 (2017).
- [28] J.R. Dyer. Applications of absorption spectroscopy of organic compounds, Prentice-Hall, Englewood Cliffs, NJ (1965).
- [29] T.M.A. Ismail, A.A. Saleh, M.A. El Ghamry. *Spectrochim. Acta A Mol. Biomol. Spectrosc.*, **86**, 276 (2012).
- [30] S. Sarkar, K. Dey, S. Biswas, B.B. Bhaumik. *J. Coord. Chem.*, **60**, 1143 (2007).
- [31] A.N.M.A. Alaghaz, M.E. Zayed, S.A. Alharbi, R.A.A. Ammar, A. Chinnathambi. *J. Mol. Struct.*, **1087**, 60 (2015).
- [32] Z. Khanam, C.S. Wen, I.U. Bhat. *J. King Saud Uni.*, **27**, 23 (2015).
- [33] D.S. Raja, S.P. Bhuvanesh, K. Natarajan. *J. Biol. Inorg. Chem.*, **17**, 223 (2012).
- [34] Y. Liu, W. Mei, J. Lu, H. Zhao, L. He, F. Wu. *J. Coord. Chem.*, **61**, 3213 (2008).



- [35] G. Yang, J.Z. Wu, L. Wang, L.N. Ji, X. Tian. *J. Inorg. Biochem.*, **66**, 141 (1997).
- [36] B. Tweedy. *Phytopathology*, **55**, 910 (1964).
- [37] L.H. Abdel-Rahman, A.M. Abu-Dief, R.M. El-Khatib, S.M. Abdel-Fatah. *Bioorg. Chem.*, **69**, 140 (2016).
- [38] A.D.M. Mohamad, M.J.A. Abualreish, A.M. Abu-Dief. *J. Mol. Liq.*, **290**, 111162 (2019).
- [39] L.H. Abdel-Rahman, M.S. Adam, A.M. Abu-Dief, H. Mostafa, M.T. Basha. A.S. Aboraia, B.S. Al-Farhan, H.S. Ahmed. *Appl. Organomet. Chem.*, **32**, e4943 (2018).
- [40] G. Feng, J.C. Mareque-Rivas, N.H. Williams. *Chem. Commun.*, **17**, 1845 (2006).
- [41] L.M. Gaetke, C.K. Chow. *Toxicology*, **189**, 147 (2003).
- [42] S. Ramakrishnan, E. Suresh, A. Riyasdeen, M.A. Akbarsha, M. Palaniandavar. *Dalton Trans.*, **40**, 3245 (2011).